

A Frequency-Selective Broadband Low-Noise Amplifier With Double-Loop Transformer Feedback

Sumit Bagga, *Member, IEEE*, Andre L. Mansano, *Student Member, IEEE*, Wouter A. Serdijn, *Fellow, IEEE*, John R. Long, *Member, IEEE*, Koen Van Hartingsveldt, *Member, IEEE*, and Kathleen Philips, *Member, IEEE*

Abstract—A frequency-selective, power-to-current (P-I) broadband low-noise amplifier (FS-LNA) is presented. The use of global and/or local feedback in tandem is investigated, where monolithic transformers realize the feedback loops. Superior performance is realized when global and local feedbacks are interwound. A cascode gain stage with a current-to-current positive feedback loop to boost the power gain and a current-to-current negative feedback loop for impedance and/or noise matching is implemented in 90 nm RF-CMOS. The FS-LNA also provides at least 20 dB RF signal rejection at frequencies below the L-band (includes GPS and GSM carriers). The measured gain, noise figure and 1-dB gain compression point of the LNA from 3.5–9.25 GHz are 15 ± 3 dB, 2.4 ± 0.8 dB and -17.5 ± 2.5 dBm, respectively. The chip area of the LNA is 0.7×0.8 mm². The FS-LNA consumes 9.6 mW from a 0.8 V power supply. It is most suitable for sub-1 V single-cell integrated radios and can be used for multiband/multistandard wireless technologies, such as broadband impulse-radio ultra-wideband (IR-UWB) and frequency modulated (FM) UWB.

Index Terms—Broadband, frequency selectivity, low-noise amplifier, monolithic transformers, transformer feedback.

I. INTRODUCTION

MULTIBAND/MULTISTANDARD concepts have spurred considerable interest in broadband RFIC design. However, the traditional approach to RFIC design is playing catch-up, particularly to the design requirements (e.g., complexity, cost and power consumption) associated with these new broadband wireless standards and applications. Broadband low-noise RF amplifiers (LNAs) are thus required for multiband/multistandard RF receiver front-end architectures. As the first block of the receiver chain, a broadband LNA must offer robust RF performance, such as gain, power consumption, input power matching, noise figure, signal distortion and group delay (linear phase response) over several gigahertz of signal bandwidth.

Manuscript received June 28, 2013; revised September 19, 2013; accepted October 22, 2013. Date of publication January 09, 2014; date of current version May 23, 2014. This work was supported in part by Delft University of Technology, The Netherlands and in part by Conselho Nacional de Desenvolvimento Científico e Tecnológico (CNPq), Brazil. This paper was recommended by Associate Editor N. M. Neihart.

S. Bagga is with the ERL/DIMES, Delft University of Technology, 2628 CD Delft, The Netherlands, and also with the DFchip, Brasilia-DF, Brazil (e-mail: sumit.bagga@ieee.org).

A. L. Mansano, W. A. Serdijn, and J. R. Long are with the ERL/DIMES, Delft University of Technology, 2628 CD Delft, The Netherlands (e-mail: serdijn@ieee.org).

K. Van Hartingsveldt is with Catena, Elektronikaweg 40, 2628 XG Delft, The Netherlands.

K. Philips is with the IMEC-NL, Holst Centre, 5605 KN Eindhoven, The Netherlands.

Digital Object Identifier 10.1109/TCSI.2013.2295010

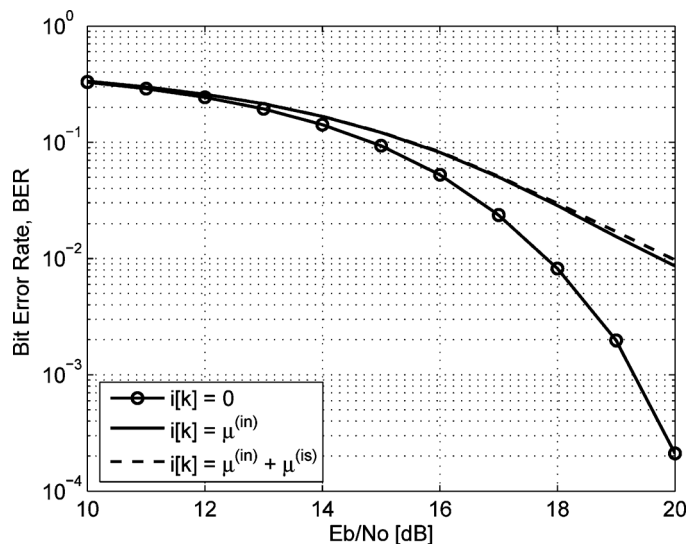


Fig. 1. Effect of NBI correlation terms on the BER for an average signal-to-interference ratio (C/I) of -10 dB, where $C/I = E_b/(T_b P_i)$. T_b is the bit duration, E_b is the energy per bit of the signal and P_i is the power of the narrowband interferer.

In addition to the aforementioned parameters, frequency selectivity is another important design characteristic in wireless broadband systems (e.g., ultra-wideband), which not only transmit at low power spectral densities, but also share scarce spectrum resources with existing narrowband systems. Studies show that non-coherent receiver types (e.g., auto-correlation receivers (ACRs)), are especially susceptible to narrowband interference (NBI) [1], [2]. In the case of an ACR, the narrowband interference term, $i(t)$ is expressed as

$$i(t) = \mu^{(ii)} + \mu^{(in)} + \mu^{(is)} \quad (1)$$

where $\mu^{(ii)}$, $\mu^{(in)}$ and $\mu^{(is)}$ are the interference-interference, interference-noise and interference-signal correlation terms, respectively [3]. Here, NBI is modeled by a single tone sinusoidal interferer.

Through digital signal processing, we can reduce $\mu^{(ii)}$ by several orders of magnitude, unlike terms $\mu^{(in)}$ and $\mu^{(is)}$, which may not be removed completely. These unwanted interference terms must be suppressed in the analog RF front-end to limit BER degradation. Fig. 1 shows that the dominant factor in bit error rate (BER) degradation is the interference-noise term.

To improve the RF front-end's sensitivity, a passive (lossy) filter (e.g., as designed in [4]) is often placed at the receiver's

TABLE I
P-I FS-LNA TARGET SPECIFICATIONS.

Parameter	Target Specification
Bandwidth	3.1-10.6 GHz
Forward Trans. Coeff. (S_{21})	≥ 15 dB
Reverse Trans. Coeff. (S_{12})	≤ -25 dB
Input Reflection Coeff. (S_{11})	≤ -10 dB
Output Reflection Coeff. (S_{22}^\dagger)	n.a.
Noise Figure	≤ 2 dB
1-dB Comp. Pt. (P_{-1dB})	≥ -20 dBm
Notch [†]	≥ 20 dB
Group Delay (GD) Variation	≤ 10 % of GD
Signal Distortion	$\leq 5\%$
Power DC	≤ 10 mA (at 0.8 V)

[†] Out-of-band: L-band.

[‡] As this P-I FS-LNA is power-to-current configured, the S_{22} is close to zero.

input in order to reject out-of-band interferers. The drawback of this approach is that the insertion loss of the filter adds directly to the overall noise figure of the receiver. An alternative solution is to distribute the required interference rejection in the RF front-end by means of a notch antenna that offers attenuation in the passband [5], [6] in conjunction with a frequency-selective broadband LNA designed to reject out-of-band signals. The frequency-selective broadband LNA is the topic of this work.

In amplifiers, negative feedback promotes insensitivity to process and supply variations, stabilization of gain, lower distortion, larger bandwidth (at the expense of gain), and orthogonal noise and impedance matching in amplifiers [7], [8]. In principle, a single current-to-current (I-I) negative feedback loop together with a transistor's transconductance (voltage-to-current transfer), g_m , can define its input impedance. For impedance matching at the input and output ports of an amplifier, double-loop feedback configurations, such as power-to-current (P-I), current-to-power (I-P), power-to-voltage (P-V), voltage-to-power (V-P) and power-to-power (P-P) are used. A power-to-current configuration is the preferred choice, as the proposed FS-LNA is to be interfaced with a mixer or an IF filter.

After taking into account all the information presented in the preceding paragraphs, a frequency-selective, power-to-current broadband LNA topology with double-loop transformer feedback is chosen. The FS-LNA is applicable in multiband/multistandard RF front-end architectures. The FS-LNA is implemented in a standard 90 nm CMOS process and operates from a 0.8 V power supply, and therefore, is most suitable for sub-1 V single-battery integrated radios. A low noise figure, broadband gain and input power matching without the need of a lossy input filter, is achieved through the use of positive and negative double-loop transformer feedback networks via on-chip transformers. The target specifications of the P-I FS-LNA are listed in Table I. Transformer feedback is used to realize broadband gain, low noise (as transformer feedback does not add thermal noise [9]), a well-defined broadband input match (for maximum power transfer) and moderate-to-high linearity.

The paper is organized as follows. As we have learned from our previous design experiences, the design of a broadband LNA with limited open-loop gain requires multiple feedback loops to form a well-defined input impedance [3], [10]. Thus, in Section II, we present and compare two topologies of the P-I FS-LNA. The first of the two topologies comprises I-I/V-V global transformer feedback loops, where the second design effectively combines global and local I-I transformer feedback loops. Because of the latter's superior performance and relative ease of design, measurement results are presented only for the LNA employing global/local transformer feedback (Section III). Conclusions are drawn in Section IV.

II. LOW-NOISE AMPLIFIERS WITH DOUBLE-LOOP TRANSFORMER FEEDBACK

We first present the P-I FS-LNA comprising only global feedback loops. Its shortcomings are highlighted. Then a new P-I FS-LNA with interwound global and local feedback loops is proposed.

A. Prior Art: P-I FS-LNA With Global Double-Loop (I-I/V-V) Transformer Feedback

The P-I LNA topology with double-loop transformer feedback (see Fig. 2) is a potential candidate for broadband radios [11]. This P-I LNA comprises a single common-source stage (M_1) followed by a common-gate (CG) stage (M_2). Transformers T_1 and T_2 realize the negative current-to-current (for impedance matching) and positive voltage-to-voltage (for gain boosting) transformer feedback loops, respectively.

The positive feedback loop works as follows: the intermediate voltage (v_{s_2} at source of M_2) is sensed through the primary winding of T_2 and added in series (through the secondary) to the input voltage of the LNA, thereby effectively increasing the transconductance of the amplifier to G_m . The impedance $1/g_{m_2}$ seen at the input (source terminal) of M_2 controls the positive feedback. If the amount of positive feedback is made constant, then the topology of the LNA can be reduced to a single-stage common-source amplifier. As for the negative feedback loop, the intermediate current ($i_{p,1}$) is sensed by the primary winding T_1 and added (through the secondary) to the gate of M_1 , in order to create a well-defined input impedance, Z_i .

To obtain a low noise figure (≤ 2 dB) and a power gain ≥ 15 dB, transistor M_1 is properly dimensioned for a maximum DC bias current of 10 mA (as per target specification). The noise contribution from M_2 is negligible as the channel noise, i_{nd_2} of M_2 at the input of the CG-stage input is $i_{nd_2}(1 - 1/\beta_{i_2})$, where β_{i_2} is the current transfer of the CG-stage and is close to 1. For frequency selectivity, a series LC resonant network formed with the secondary winding ($T_{s,1}$ of T_1) and coupling capacitor C_1 places a notch in the stop-band (at L-band).

The P-I FS-LNA with global double-loop (I-I/V-V) transformer feedback was measured in TSMC's 90 nm RF-CMOS technology. This design did meet most of the target specifications, but at the same time presented several shortcomings, such as:

- 1) Gain: in [11], transformer T_1 was assumed to be a perfectly-coupled transformer in order to simplify the derivation for the gain (power). Taking into account the non-ide-

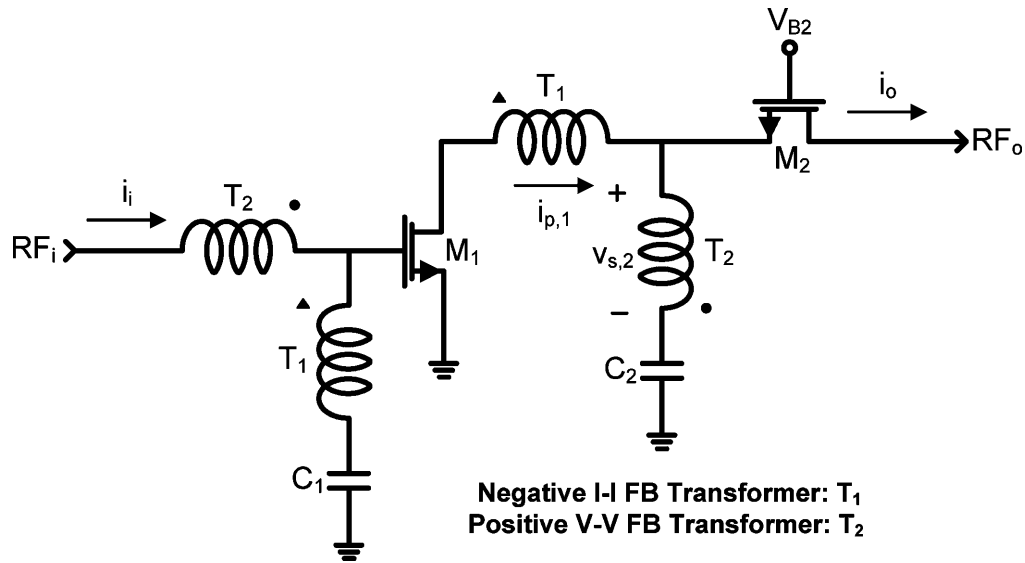


Fig. 2. Schematic of the P-I LNA core with (negative I-I and positive V-V) transformer feedback loops.

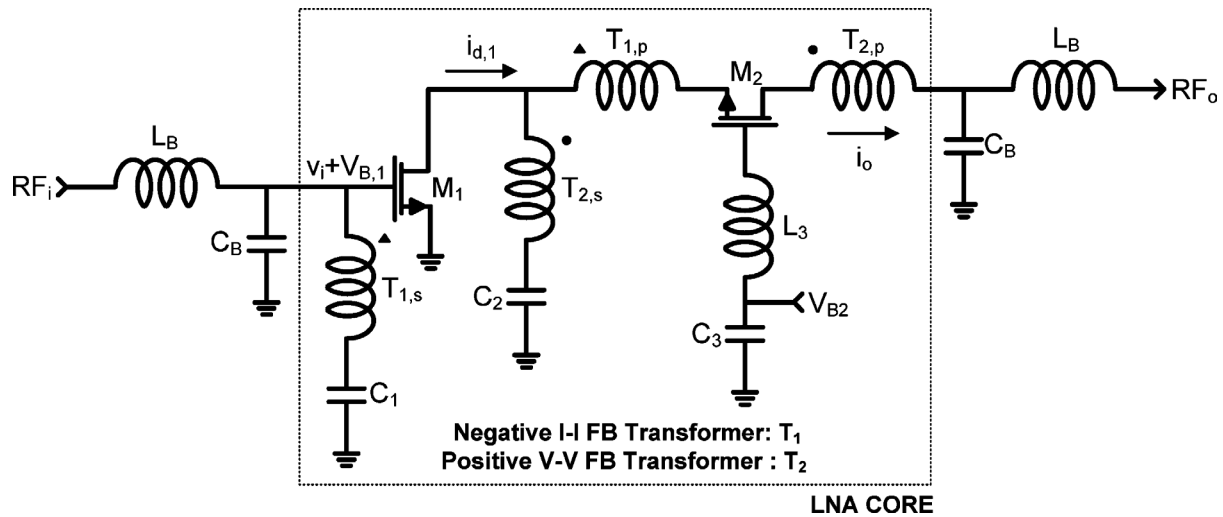


Fig. 3. Schematic of the P-I LNA with double-loop (negative I-I and positive I-I) transformer feedback.

alities of T_1 , the actual gain can be much less than the theoretical gain.

- 2) Noise figure: higher noise figure as a result of the global positive feedback loop (i.e., output-to-input transfer via windings of transformer T_2).
- 3) Input matching: the input impedance is susceptible to both the self-inductances and the effective turn ratios of the double-loop transformers.

We will now show that all these issues can be easily resolved by substituting the global V-V positive feedback loop with a local I-I positive feedback loop.

B. P-I FS-LNA With Global/Local Double-Loop (I-I/I-I) Transformer Feedback

The P-I FS-LNA as shown in Fig. 3 [12] also comprises a single common-source stage (M_1) and two feedback networks made up of current-to-current transformers followed by a common-gate stage (M_2). Transformer T_1 has a concentric configuration with weak mutual coupling and T_2 has a stacked

configuration with moderate mutual coupling. Note that the primary winding $T_{2,p}$ of T_2 is connected ‘around’ M_2 . While providing a high output impedance node, transistor M_2 also isolates the primary windings $T_{1,p}$ and $T_{2,p}$ of transformers T_1 and T_2 , respectively. To minimize the noise figure and maintain high gain, transistor M_1 is properly dimensioned for a maximum DC bias current of 10 mA (as per target specification).

With a single (local) I-I positive feedback loop at its input, the input impedance of the LNA is made less susceptible to the turns ratio and coupling coefficient of the power gain boosting transformer T_2 . The positive feedback loop works as follows: the output current (i_o) is sensed by $T_{2,p}$ of T_2 and added to the drain current ($i_{d,1}$) of M_1 , thereby boosting the overall transconductance ($G_m \triangleq i_o/v_i$) without increasing the bias current. As for the negative feedback loop [4], the output current (and not the intermediate current as seen in the previous topology) is sensed by $T_{1,p}$ of T_1 and added to the gate of M_1 .

Inductance L_3 (300 pH) resonates with the parasitic capacitances of M_2 to compensate for the high frequency gain roll-off.

Higher values of L_3 can cause instability and thus the chosen value must be properly modeled. The bondwires and bondpads are modeled using L_B (500 pH) and C_B (150 fF), respectively.

Transformer non-idealities are neglected to simplify the derivation for G_m , power gain (G_p) and Z_i . Note that the current sensed through the primary of T_1 is equal to the output current. It then follows:

$$G_m = \frac{g_{m_1}}{1 - \frac{k_2}{n_2}} \quad (2)$$

where g_{m_1} is the intrinsic transconductance of the first stage transistor M_1 , k_2 is the coupling coefficient and n_2 is the turns ratio of transformer T_2 .

The power gain is expressed as:

$$G_p = \left(\frac{n_1}{k_1}\right) \left(\frac{g_{m_1}}{1 - \frac{k_2}{n_2}}\right) Z_L \quad (3)$$

where n_1/k_1 is the transfer ratio, k_1 is the coupling coefficient and n_1 is the turns ratio of transformer T_1 , and Z_L is the load impedance.

For broadband applications, modeling and understanding the interplay between the transformers to achieve an input match of 50Ω is required. From the individual equations of the two transformer feedback loops, the input impedance of the LNA can be approximated as:

$$Z_i = \left(\frac{n_1}{k_1}\right) \left(\frac{1 - \frac{k_2}{n_2}}{g_{m_1}}\right). \quad (4)$$

We know from literature that the effective turns ratio of a monolithic transformer is limited by the coupling coefficient and its parasitics. This geometric bottleneck is solved by designing a transformer with a low coupling coefficient and a large self-inductance ratio between the secondary and the primary windings. However, with a low coupling coefficient, the transformer's electrical performance is lowered, and thus, the introduction of a positive feedback loop provides a greater degree of control over the input impedance, while boosting the power gain. To ensure unconditional stability, the negative feedback loop is the dominant loop of the LNA.

A large ratio between the winding self-inductances (of T_1) creates a geometric bottleneck. To maximize the effective turns ratio, transformer T_1 is constructed using a concentric geometric configuration. For the purposes of maintaining stability, the stacked transformer T_2 must realize a physical turns ratio ≥ 1 . The two transformers are modeled using ADS Momentum. For frequency-selectivity, a series LC resonant network formed (with $T_{s,1}$ and coupling capacitor C_1) places a notch in the stop-band (at L-band).

The positive feedback transformer T_2 boosts the overall transconductance, g_{m_1} to G_m by a factor (G_m/g_{m_1}) of 2.25 ± 0.75 (see Fig. 4), thereby boosting the power gain (3). As $T_{2,p}$ is partially outside the negative feedback loop formed by T_2 , the dynamics of the interlocked negative and positive feedback loops must be properly simulated to ensure unconditional stability.

High power gain and a broadband input match of 50Ω is realized by setting the effective turns ratio of transformer T_1 (n_1/k_1) sufficiently large (≥ 8) and that of transformer $T_2 \geq 1$.

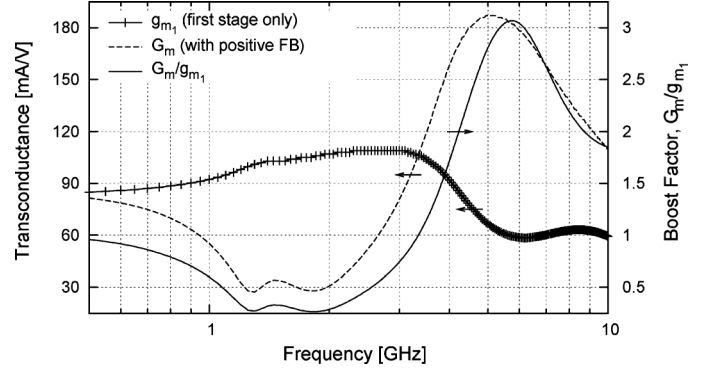


Fig. 4. Simulated transconductance 'boosting' with a positive I-I feedback loop.

TABLE II
CONCENTRIC AND STACKED TRANSFORMER PARAMETERS.

Trans.	k	L_s (nH)	L_p (nH)	N^\dagger	$Q_{s/p}^\ddagger$
T_1^\S	0.3	2.1	0.33	8.4	23/19
T_2^\S	0.65	1.2	1.5	1.4	21/18

† Effective turns ratio, $N = (n/k) = \frac{1}{k} \sqrt{\frac{L_s}{L_p}}$.

‡ Q-factor of T_1 and T_2 simulated at 6.5 GHz.

§ OD of T_1 is $250 \times 325 \mu\text{m}^2$ and T_2 is $225 \times 225 \mu\text{m}^2$.

This sets the overall transconductance of the LNA (G_m) close to 150 mA/V, which is at least a factor 1.5 times that of g_{m_1} .

To realize a power gain ≥ 15 dB, an input impedance of 50Ω and a noise figure ≤ 2 dB, we use the transformer specifications as shown in Table II.

For the noise analysis, we will derive an expression for the total equivalent noise power spectral density (PSD), $S_{v_{n,eq}}^*$. Transformer parasitics will be neglected to simplify the analysis. Thus, after shifting all the noise sources (gate resistance noise voltage of M_1 and channel noise current of M_1 and M_2), the equivalent input noise ($v_{n,eq}$ and $i_{n,eq}$) is given by

$$\begin{aligned} v_{n,eq} &= v_{g_1} + \frac{i_{nd_1}}{g_{m_1}} + \frac{i_{nd_2}^*}{N_2 g_{m_1}} - \frac{i_{nd_2}^*}{G_m} \\ i_{n,eq} &= \frac{i_{nd_1}}{\beta_{i_1}} + \frac{i_{nd_2}^*}{N_2 \beta_{i_1}} - \frac{i_{nd_2}^*}{\beta_i} \end{aligned} \quad (5)$$

where v_{g_1} is the noise voltage resulting from the gate resistance r_{g_1} of M_1 , $i_{nd_2}^*$ is the output referred channel noise of M_2 ($i_{nd_2}(\beta_{i_2} - 1)$), where β_{i_2} is the current transfer of the CG-stage. The current transfers of the CS-stage and the LNA are β_{i_1} and β_i , respectively, and are expressed as

$$\begin{aligned} \beta_{i_1} &= N_1(1 - N_2^{-1}) \\ \beta_i &= N_1. \end{aligned} \quad (6)$$

We transform $i_{n,eq}$ to a voltage source in series with $v_{n,eq}$ to derive $v_{n,eq}^*$.

$$v_{n,eq}^* = v_{n,eq} + i_{n,eq}(Z_s + r_{g_1}) \quad (7)$$

where Z_s is the source impedance.

When substituting for G_m , β_{i_1} , β_i , and combining all the noise sources, the resulting expression for the total equivalent noise PSD ($S_{v_{n,eq}^*}$) is too complex to evaluate. Instead, intuitively we determine which terms can be safely neglected. As

TABLE III
DESIGN SUMMARY.

Performance Parameter	LNA 1 [†]	LNA 2 [‡]
Operation at Sub-0.5 V	+++	n.a.
Operation at Sub-1 V	+++	+++
Power Gain	+	+++
Impedance Matching	+	+++
Noise Figure	++	+++

[†] LNA with global I-I/V-V feedback loops.

[‡] LNA with global/local I-I feedback loops.

$\beta_{i_1}^2$ and $\beta_{i_2}^2$ are much larger than 1 (for $f \ll f_T$), term $i_{n,eq}(Z_s + r_{g_1})$ is neglected. Moreover, as $i_{nd_2}^*/N_2 g_{m_1} \gg i_{nd_2}^*/G_m$, the latter term $i_{nd_2}^*/G_m$ can be also neglected. Upon simplification the total equivalent noise PSD is expressed as

$$S_{v_{n,eq}}^* = 4kT \left(r_{g_1} + \left(\frac{\gamma}{\alpha} \right) \left(\frac{1 + (\Gamma)(\beta_{i_2} - 1)^2 N_2^{-2}}{g_{m_1}} \right) \right) \quad (8)$$

where γ/α is a complex function. Its value is determined from the transistor parameters and bias conditions. For short-channel devices, it is usually less than 1. Variable Γ denotes g_{m_2}/g_{m_1} .

At low frequencies, β_{i_2} is close to 1. At higher frequencies, even if β_{i_2} is less than 1, the term $(\beta_{i_2} - 1)^2 N_2^{-2} \ll 1$. When $g_{m_1} \approx g_{m_2}$, (8) simplifies to

$$S_{v_{n,eq}}^* = 4kT \left(r_{g_1} + \frac{\gamma}{\alpha g_{m_1}} \right). \quad (9)$$

From (9), and confirmed via simulations, it follows that in order to achieve the best compromise between noise figure and power consumption, the input stage noise contribution can be minimized by maintaining a high current efficiency (i.e., transconductance to current ratio). As the bias current is fixed per specifications, a higher transconductance of the first stage translates into lower noise contribution of subsequent stages. The gate resistance noise of M_1 can be reduced through proper dimensioning.

We can now compare the characteristics of the two P-I FS-LNA designs (see Table III). For sub-0.5 V operations, the LNA with global feedback is more suitable as the second (common-gate) stage is only required for positive feedback control. However, when benchmarked against all the specifications (as stated in Table I), the P-I FS-LNA with global and local I-I feedback loops is superior.

III. MEASUREMENT RESULTS

The LNA is mounted on a double-sided, copper-clad high frequency laminate (see Fig. 5). It sits in a cavity and is wire-bonded to input/output 50 coplanar waveguide (CPW) feedlines. The bondwire interconnect lengths are less than 300 μm corresponding to approximately 300 pH series inductances to the input/output of the LNA. The measurements are referenced to the PCB interface.

The microphotograph of the P-I FS-LNA fabricated in IBM's 90 nm RF-CMOS process is shown in Fig. 6. The chip area is 0.56 mm^2 (0.7 \times 0.8 mm^2) including all bondpads. The active area is approximately 0.3 mm^2 . All inductors, transformers and

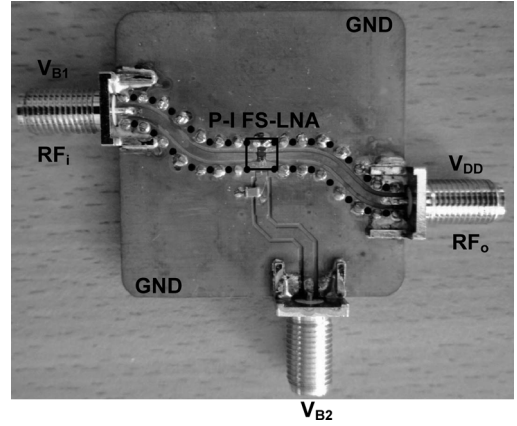


Fig. 5. PCB with the frequency-selective P-I LNA.

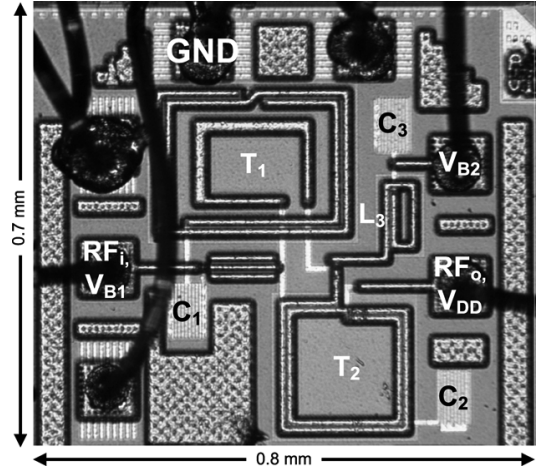


Fig. 6. Microphotograph of the frequency-selective P-I LNA in 90 nm CMOS.

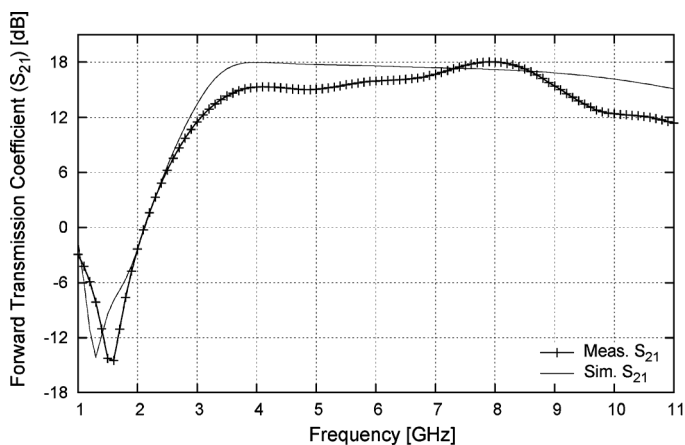
metal-insulator-metal (MiM) capacitors are implemented in the top metallization layers.

The measured and simulated results for the forward transmission (S_{21}) and reflection (S_{11}) coefficients are shown in Fig. 7. In the passband (3.25–9.5 GHz), the power gain is 15 ± 3 dB. The LNA presents at least 20 dB of rejection at frequencies below the L-band (which includes GPS and GSM carriers). The transconductance of the amplifier and the transformer parameters (i.e., self-inductances of the windings, physical turns ratio and coupling coefficient) set the input impedance of the LNA to approximately 50 Ω . The measured S_{11} varies from -7 (only at higher frequencies) to -16 dB over the required bandwidth as illustrated in Fig. 7.

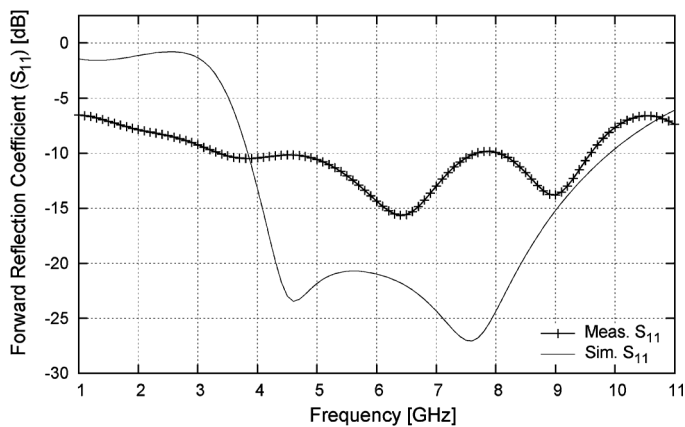
The measured reverse transmission coefficient (isolation), $S_{12} \leq -20$ dB (see Fig. 8). Discrepancy in S_{12} is most likely a result of unwanted parasitic feedback (i.e., coupling between transformer windings of T_1 and T_2).

The noise figure is shown in Fig. 9. As expected, the noise figure (2.4 ± 0.8 dB) is inversely proportional to the gain.

In broadband amplifier design, transformer feedback increases linearity without increasing thermal noise. The 1-dB compression point, $P_{-1\text{dB}}$ is one appropriate measure of the linearity for broadband circuits to predict low-level intermodulation effects. The $P_{-1\text{dB}}$ remains relatively constant (-17 ± 2.5 dBm) throughout the required frequency range as shown in Fig. 10



(a)



(b)

Fig. 7. Forward transmission (a) and reflection coefficients (b) of the frequency-selective P-I LNA (after de-embedding). Gain peaking occurs from 7 to 9 GHz instead of 8 to 10 GHz as a result of improper modeling of the self-inductance L_3 (see Fig. 3).

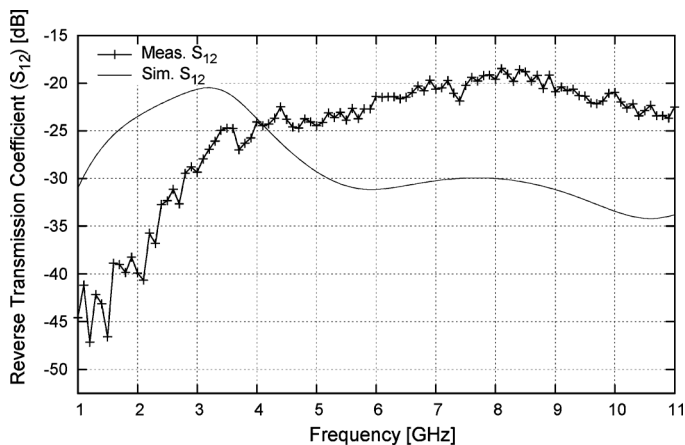


Fig. 8. Measured and simulated reverse transmission coefficient of the frequency-selective P-I LNA.

The input-inferred third-order intercept point (IIP3) is another important linearity figure of merit [13]. The IIP3 curve (specified at 10 MHz offset) for the P-I FS-LNA is shown in Fig. 11. Simulated and measured results compare well. At offset frequencies of 250 MHz and 500 MHz, the IIP3 ranges from approximately -17 to -13 dBm, with an average value of -15 dBm.

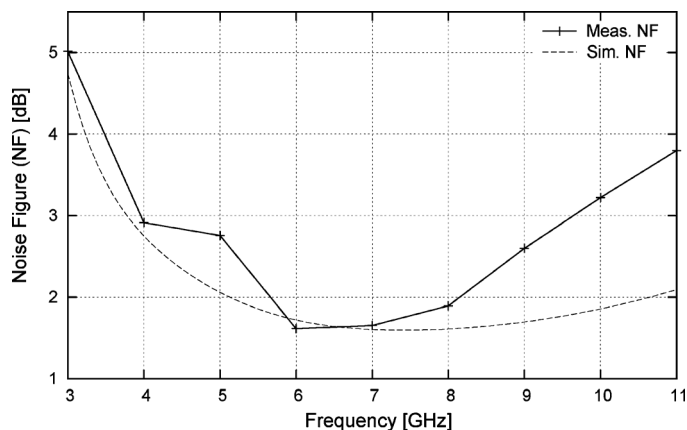


Fig. 9. Measured and simulated noise figure of the frequency-selective P-I LNA.

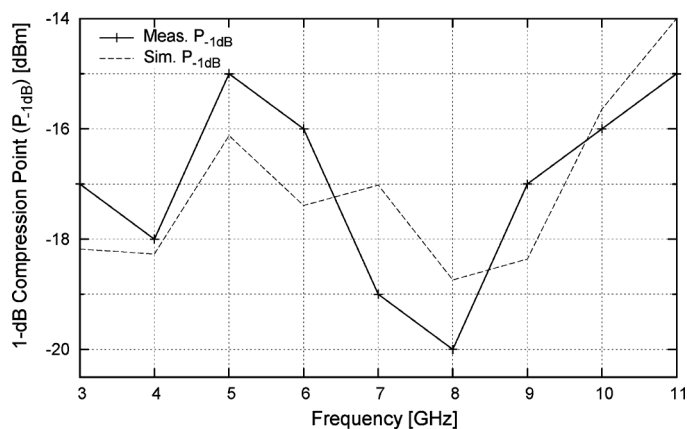


Fig. 10. Measured and simulated 1-dB compression point of the frequency-selective P-I LNA.

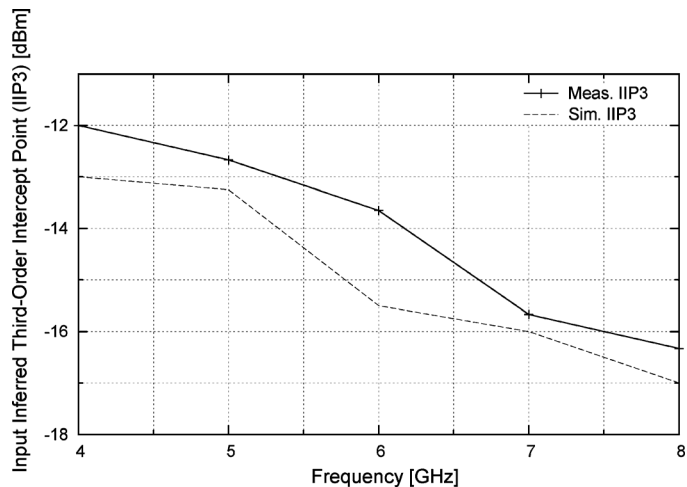


Fig. 11. Measured and simulated input-inferred third-order intercept point of the frequency-selective P-I LNA.

As it employs feedback, the P-I FS-LNA may be prone to instability. To verify its stability, we calculate the stability factor μ of a 2-port network [14]. This factor indicates whether or not an amplifier is unconditionally stable [15]. Only conditional stability is confirmed as $\mu < 1$ (see Fig. 12). However, when measured in a 50Ω environment, the input impedance is positive, and thus, the P-I FS-LNA with double-loop transformer feedback is conditionally stable.

TABLE IV
SUMMARY OF THE P-I FS-LNA AND COMPARISON WITH PREVIOUSLY PUBLISHED DESIGNS.

Specifications	This work	[10]	[16]	[17]	[18]	[19]	[20]	[21]
BW (GHz)	3.5-9.25	3.25-10.25	3.1-10.6	3.0-10	2.4-9.5	3-10	3.4-11.4	0.2-5.2
S_{21} (dB)	15 \pm 3	14.5 \pm 2.5	15.3 \pm 2.2	19 \pm 2	7.8 \pm 1.5	18.5 \pm 1.7	14.75 \pm 1.25	15.6*
Notch (dB)	≥ 20 at 1.5 GHz	20 at 5.25 GHz	n.a.	n.a.	n.a.	n.a.	n.a.	n.a.
S_{11} (dB)	(-16) to (-8)	(-16) to (-10.5)	(-25) to (-8.6)	(-14) to (-9)	(-38) to (-15)	< -7.2	(-40) to (-10)	< -10
S_{12} (dB)	< -20	< -36	< -25	n.a.	< -35	< -37	< -45	n.a.
GD (ps)	330 \pm 40 [†]	225 \pm 125	102.5 \pm 27.5	n.a.	187.5 \pm 62.5	n.a.	n.a.	n.a.
NF (dB)	2.4 \pm 0.8	2.9 \pm 0.8	2.51 \pm 0.47	3.4 \pm 0.85	6.6 \pm 2.6	2.45 \pm 0.65	4.55 \pm 1.45	< 3.5
IIP3 (dBm)	(-16.3) to (-12) [‡]	(-9) to (-1.8)	(-7.2) to (-4.3)	(-5.5) to 3	(-8.2) to (-5.6)	2.1 (6 GHz)	-7 (6 GHz)	> 0
V_{DD}/P (V/mW)	0.8/9.6	1.2/15	1.2/9	3.3/30	1.8/9	3.3/26	1.8/11.9	1.2/21
Area (mm ²)	0.56	1.68	0.87	1.8	1.1	0.72	1.2	0.009
Tech. (nm)	C-90	C-130	C-130	SiGe-180	C-180	SiGe-180	C-180	C-65

*Voltage gain; [†]Including test fixture; [‡]Measured IIP3 from 4 to 8 GHz.

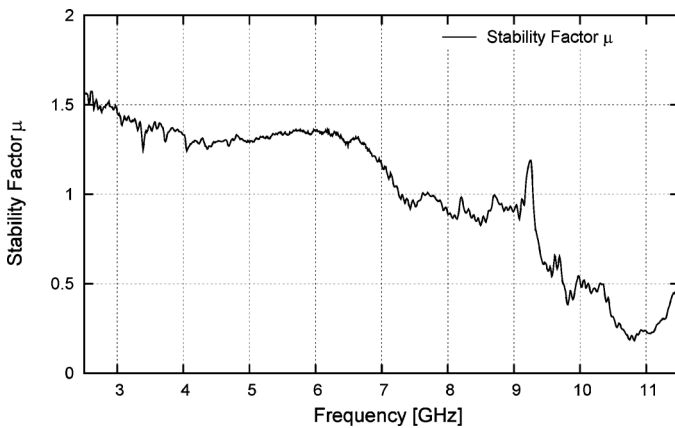


Fig. 12. Measured stability factor μ of the P-I FS-LNA (with test fixture).

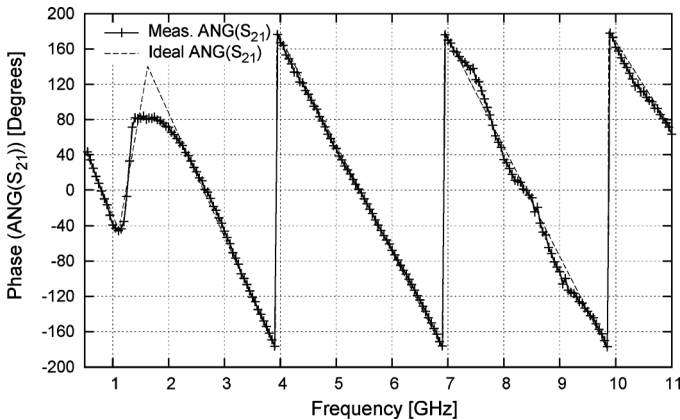
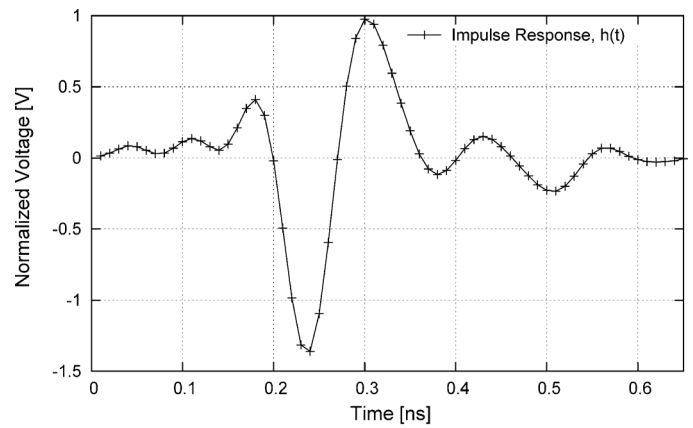


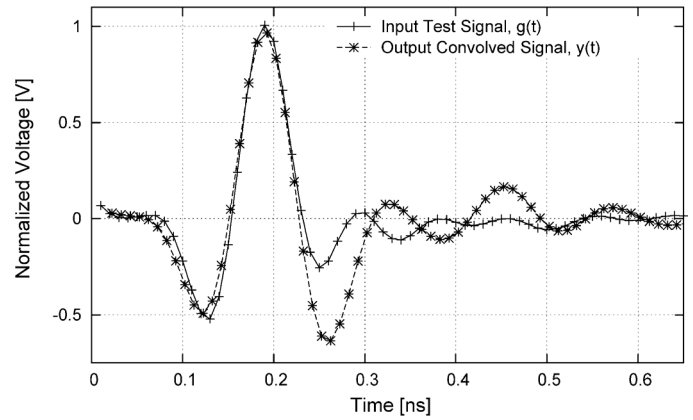
Fig. 13. Measured and simulated phase response of the P-I FS-LNA (with test fixture).

Especially for circuits with filter-like characteristics, time and frequency domain analyses are extremely helpful in visualizing signal distortion. In the frequency domain, a linear phase/constant group delay response is a requirement in broadband amplifiers. The measured phase response of the P-I FS-LNA is shown in Fig. 13. At the notch (1.5 GHz), the LNA's phase response exhibits a phase jump of approximately 125°.

Fig. 14(a) illustrates the normalized measured impulse response, $h(t)$ of the P-I FS-LNA (i.e., inverse fast Fourier transform (IFFT) of S_{21}). Fig. 14(b) shows an ideal input test signal (i.e., with a band-limited (brick-wall) frequency spectrum from



(a)



(b)

Fig. 14. Time domain analysis. (a) Measured impulse response $h(t)$ (IFFT of S_{21}) of the frequency-selective P-I LNA. (b) Output signal derived by convolving an input test signal $g(t)$ with the LNA's impulse response. It is to be noted that the output signal is normalized, time-shifted and inverted.

3–11 GHz), $g(t)$ and an output signal, $y(t)$ (i.e., $g(t)*h(t)$). This convolved signal shows some distortion in the form of ringing because of the non-linear phase response between 7–9 GHz.

Table IV compares the proposed frequency selective LNA to recently published broadband LNAs in standard CMOS and SiGe HBT technologies. The P-I FS-LNA with double-loop (I-I/I-I) transformer feedback demonstrates superior design characteristics, such as a smaller silicon footprint, is capable of oper-

ating from a sub-1 V power supply, is not technology dependent (as a result of feedback) and incorporates filter-like characteristics required to provide excellent out-of-band rejection.

The P-I FS-LNA shows similar characteristics to those presented in [16] (as the authors also employ transformer feedback), but superior to [18] and [20], where the latter two amplifiers are also designed in CMOS technology. The amplifiers in [17] and [19] exhibit higher power gains (≥ 20 dB) as the transconductance (for the same bias current) of a SiGe HBT is considerably higher as compared to a MOS transistor. We exploit positive feedback to maintain a power gain ≥ 15 and a NF around 2 dB.

IV. CONCLUSION

Two topologies of broadband low-noise amplifiers are presented. The power-to-current configured, frequency-selective LNA with double-loop (global and local) transformer feedback is shown to be the better design and is fabricated in IBM's 90 nm RF-CMOS technology. The feedback loops are realized using on-chip concentric and stacked transformer configurations. A notch ≥ 20 dB is placed in the stopband to suppress narrow-band interferers below the L-band (which includes GPS and GSM carriers). The measured power gain of the P-I FS-LNA is 15 ± 3 dB. The LNA's noise figure (2.4 dB) and the 1-dB compression point (-17.5 dBm) show a ± 0.8 dB and ± 2.5 dBm variation from 3.25–9.5 GHz, respectively. It consumes 9.6 mW from a 0.8 V supply.

ACKNOWLEDGMENT

The authors thank IBM Microelectronics for fabrication support.

REFERENCES

- [1] A. Swami, B. Sadler, and J. Turner, "On the coexistence of ultra-wideband and narrowband radio systems," in *Proc. Military Commun. Conf., MILCOM*, 2001, vol. 1, pp. 16–19.
- [2] M. Pausini, "Autocorrelation receivers for ultra wideband wireless communications," Ph.D. dissertation, Delft Univ. Technology, Delft, The Netherlands, 2007.
- [3] S. Bagga, "Ultra-wideband transceiver circuits and systems," Ph.D. dissertation, Delft Univ. Technology, Delft, The Netherlands, 2009.
- [4] S. Bagga, Z. Irahhtauten, W. A. Serdijn, J. R. Long, and J. Pekarik, "An UWB transformer-coupled orthonormal state space band-reject filter in 0.13 μm CMOS," in *Proc. IEEE Eur. Solid-State Circuits Conf.*, Sep. 2008, pp. 298–301.
- [5] H. G. Schantz, G. Wolenc, and E. M. Myska, III, "Frequency notched UWB antennas," in *Proc. IEEE Conf. Ultra Wideband Syst. Technol.*, Nov. 2003, pp. 214–218.
- [6] S. Y. Suh, W. L. Stutzman, W. A. Davis, A. E. Waltho, K. W. Skeba, and J. L. Schiffer, "A UWB antenna with a stop-band notch in the 5 GHz WLAN band," in *Proc. IEEE/ACES Int. Conf. Wireless Commun. Appl. Computational Electromagn.*, Apr. 2005, pp. 203–207.
- [7] X. Li and W. A. Serdijn, "On the design of broadband power-to-current low noise amplifiers," *IEEE Trans. Circuits Syst. I, Reg. Papers*, vol. 59, no. 3, pp. 493–504, Mar. 2012.
- [8] C. T. Fu and C. N. Kuo, "A 3–11 GHz CMOS UWB LNA using dual feedback for broadband matching," in *Proc. IEEE Radio Freq. Integr. Circuits (RFIC) Symp.*, Jun. 2007, pp. 67–70.
- [9] D. J. Cassan and J. R. Long, "A 1-V transformer-feedback low-noise amplifier for 5-GHz wireless LAN in 0.18 μm CMOS," *IEEE J. Solid-State Circuits*, vol. 38, no. 3, pp. 427–435, Mar. 2003.
- [10] S. Bagga, Z. Irahhtauten, W. A. Serdijn, J. R. Long, J. Pekarik, and H. Pflug, "A band-reject IR-UWB LNA with 20 dB WLAN suppression in 0.13 μm CMOS," in *Proc. IEEE Asian Solid-State Circuits Conf.*, Nov. 2008, pp. 449–452.
- [11] S. Bagga, "Dual-Loop Feedback Amplifying Circuit," U.S. 2011/0148527, Jun. 23, 2011.
- [12] S. Bagga, A. L. Mansano, W. A. Serdijn, J. R. Long, K. Philips, and J. Pekarik, "A frequency-selective nested dual-loop broadband low-noise amplifier in 90 nm CMOS," in *Proc. IEEE Eur. Solid-State Circuits Conf.*, Oct. 2012, pp. 121–124.
- [13] B. Razavi, *RF Microelectronics*. Englewood Cliffs, NJ, USA: Prentice-Hall, 1997.
- [14] M. L. Edwards and J. H. Sinsky, "A new criterion for linear 2-port stability using a single geometrically derived parameter," *IEEE Trans. Microw. Theory Tech.*, vol. 40, no. 12, pp. 2303–2311, Dec. 1992.
- [15] D. M. Pozar, *Microwave Engineering*. New York, NY, USA: Wiley, 1998.
- [16] M. T. Reihh and J. R. Long, "A 1.2 V reactive-feedback 3.1–10.6 GHz ultra-wideband low-noise amplifier in 0.13 μm CMOS," *IEEE J. Solid-State Circuits*, pp. 1023–1033, May 2007.
- [17] A. Ismail and A. A. Abidi, "A 3.1–10.6 GHz low-noise amplifier with wideband LC-ladder matching network," *IEEE J. Solid-State Circuits*, vol. 39, no. 12, pp. 2269–2277, Dec. 2004.
- [18] A. Bevilacqua and A. M. Niknejad, "An ultra-wideband CMOS low-noise amplifier for 3.1–10.6 GHz wireless receivers," *IEEE J. Solid-State Circuits*, vol. 39, no. 12, pp. 2259–2268, Dec. 2004.
- [19] Y. Lu, R. Krithivasan, W.-M. L. Kuo, and J. D. Cressler, "A 1.8–3.1 dB noise figure (3–10 GHz) SiGe HBT LNA for UWB applications," in *Proc. IEEE Radio Frequency Integrated Circuits (RFIC) Symp.*, Jun. 2006, pp. 59–62.
- [20] Y.-J. Lin, S. S. H. Hsu, J.-D. Jin, and C. Y. Chan, "A 3.1–10.6 GHz ultra-wideband CMOS low noise amplifier with current-reused technique," *Microw. Wireless Component Lett.*, pp. 232–234, Mar. 2007.
- [21] S. C. Blaakmeer, E. A. M. Klumperink, D. M. W. Leenaerts, and B. Nauta, "Wideband balun-LNA with simultaneous output balancing, noise-canceling and distortion-canceling," *IEEE J. Solid-State Circuits*, vol. 43, no. 6, pp. 1341–1350, Jun. 2008.



Sumit Bagga was born in New Delhi, India, on October 31, 1977. He received the B.E. (hons.) degree in electrical engineering from Shivaji University, India, in 1999 and the M.Eng. and Ph.D. degrees in microelectronics from Universidade de Brasilia, Brazil, and Delft University of Technology, Netherlands, in 2002 and 2009, respectively.

From January 2008 to July 2009, he was appointed as an analog/RF researcher at IMEC, The Netherlands, where he took up the lead role in the design and implementation of an IEEE802.15.4a compliant RF front-end. Since 2010, he is an analog/RF design consultant with fabless design houses in Brazil and continues to be an invited research scholar at the Department of Microelectronics, Delft University of Technology. His current research interests include transceiver circuits for low-power, high-frequency, broadband integrated wireless systems for environment sensing and localization.

Dr. Bagga is co-recipient of Best Paper Award from the 2004 International Workshop on Ultra Wideband Systems (IWUWBS Joint with UWBST) in Kyoto, Japan.



Andre L. Mansano was born in Jaboticabal, Brazil, in 1982. He received the Bachelors degree in electrical engineering from the Universidade Estadual Paulista, São Paulo, Brazil, and the M.Sc. degree from the Universidade Estadual de Campinas, São Paulo, Brazil, in 2006 and 2009, respectively. In 2010 he joined Delft University of Technology, Netherlands as a guest researcher, where he is currently pursuing his Ph.D. degree.

In 2007, he joined Freescale Semiconductor Brazil as an analog/mixed-signal designer, where he designed general-purpose 8-bit and 32-bit microcontrollers. His IP portfolio mainly intended for the automotive industry, comprises power management controllers, switched-capacitor amplifiers, crystal oscillators and regulated charge pumps. He has authored four scientific publications and has been granted two patents. His research interests include wireless energy harvesting, low-power sensors, ultra-low power management techniques and broadband wireless communications.



Wouter A. Serdijn (M'98–SM'08–F'11) was born in Zoetermeer, the Netherlands, in 1966. He received the M.Sc. (*cum laude*) and Ph.D. degrees from Delft University of Technology, Delft, The Netherlands, in 1989 and 1994, respectively.

His research interests include low-voltage, ultra-low-power and ultra wideband integrated circuits and systems for biosignal conditioning and detection, neuroprosthetics, transcutaneous wireless communication, power management and energy harvesting as applied in, e.g., hearing instruments, cardiac pacemakers, cochlear implants, neurostimulators, portable, wearable, implantable and injectable medical devices and electroceuticals. He is co-editor and co-author of the books *EMI-Resilient Amplifier Circuits* (Springer 2013), *Ultra Low-Power Biomedical Signal Processing: An Analog Wavelet Filter Approach for Pacemakers* (Springer, 2009), *Circuits and Systems for Future Generations of Wireless Communications* (Springer, 2009), *Power Aware Architecting for Data Dominated Applications* (Springer, 2007), *Adaptive Low-Power Circuits for Wireless Communications* (Springer, 2006), *Research Perspectives on Dynamic Translinear and Log-Domain Circuits* (Kluwer, 2000), *Dynamic Translinear and Log-Domain Circuits* (Kluwer, 1998) and *Low-Voltage Low-Power Analog Integrated Circuits* (Kluwer, 1995). He authored and co-authored 7 book chapters and more than 250 scientific publications and presentations. He teaches Circuit Theory, Analog Signal Processing, Micropower Analog IC Design and Bioelectronics.

Dr. Serdijn received the Electrical Engineering Best Teacher Award in 2001 and 2004. He has served, a.o., as General Chair for IEEE BioCAS 2013, Technical Program Chair for IEEE BioCAS 2010 and as Technical Program Chair for IEEE ISCAS 2010 and 2012, as a member of the Board of Governors (BoG) of the IEEE Circuits and Systems Society (2006–2011), as chair of the Analog Signal Processing Technical Committee of the IEEE Circuits and Systems society, as a member of the Steering Committee of the IEEE TRANSACTIONS ON BIOMEDICAL CIRCUITS AND SYSTEMS (T-BioCAS) and as Editor-in-Chief for IEEE TRANSACTIONS ON CIRCUITS AND SYSTEMS—I: REGULAR PAPERS (2010–2011). He will be TPC Co-Chair for IEEE ISCAS 2014 and General Co-Chair for IEEE ISCAS 2015. He is an IEEE Distinguished Lecturer and a mentor of the IEEE.



John R. Long received the B.Sc. degree in electrical engineering from the University of Calgary, Calgary, ON, Canada, in 1984, and the M.Eng. and Ph.D. degrees in electronics from Carleton University, Ottawa, ON, Canada, in 1992 and 1996, respectively, with distinction.

He was employed for 10 years by Bell-Northern Research designing ASICs for Gbit/s fibre-optic transmission systems, and from 1996 to 2001 as an Assistant and then Associate Professor at the University of Toronto in Canada. Since January 2002 he has been chair of the Electronics Research Laboratory at the Delft University of Technology in the Netherlands. His current research interests include transceiver circuits for high-frequency, high-speed and low-power integrated wireless/wireline systems.

Prof. Long is Editor of the IEEE RFIC VIRTUAL JOURNAL: new on-line journal dedicated to radio-frequency circuit technologies. He is co-recipient of Best Paper Awards from the International Solid-State Circuits Conference (ISSCC) in 2000 and 2007, the RFIC Symposium in 2006 and 2012, and is a member of the technical program committee for the 2014 European Solid-State Circuits (ESSCIRC) conference.



Koen van Hartingsveldt received the M.Sc. degree in electrical engineering from the Delft University of Technology, Delft, The Netherlands, in 1999, where he is working toward the Ph.D. degree.

He currently works at Catena Microelectronics as senior design engineer in analog mixed-signal and analog RF electronics and as such he is involved in product design of fully integrated wireless transceivers for a large variety of applications, with design work on PAs, LNAs, transmit and receive chains, PLLs, high-speed low-power programmable dividers, millimeter-wave receivers.



Kathleen Philips received the M.Sc. degree in electrical engineering from the Katholieke Universiteit Leuven, Belgium, in 1995. She then joined the Mixed-Signal Circuits and Systems group of Philips Research Laboratories, Eindhoven, The Netherlands, where she designed mixed-signal CMOS circuits. For the work on sigma-delta conversion, she received the Ph.D. degree from Eindhoven University of Technology, Netherlands, in 2005.

Since 2007, she has been working in the Wireless group of the Holst Centre/IMEC, The Netherlands, where she has been working on ultra-low power radio IC design. As a principal researcher, she is now leading this activity and she is as program manager for the ultra-low power wireless program.